International Journal of Internet, Broadcasting and Communication Vol.16 No.4 181-193 (2024)
http://dx.doi.org/10.7236/IJIBC.2024.16.4.181

IJIBC 24-4-21

Design and Analysis of Propeller-Based Wall-Climbing Robot

Jihyun Ryu*, Seungho Kim*, Sungjae Park*, Dahee Lee*, Junhyuk Jo*, Dongha Shim**

**Undergraduate Student, Department of MSDE,*
Seoul National University of Science & Technology, Korea
*** Professor, Department of MSDE,*
Seoul National University of Science & Technology, Korea

*E-mail *jhryu1208@gmail.com, **dongha@seoultech.ac.kr*

Abstract

Wall-climbing robots have been safer alternatives to humans in hazardous industrial tasks. Propeller-based wall-climbing robots have gained attention because of their ability to travel on a wall surface with an arbitrary angle. In this study, the mechanical structure and thrust analysis of the robot is introduced, considering lightweight, efficient movement, and driving stability based on conventional propeller-driven wall-climbing robots. Additionally, the thrust analysis of the propeller was conducted through Computational Fluid Dynamics (CFD) simulation to enhance operational efficiency. This analysis shows that the height of the propeller from a contacting wall surface is a significant design parameter for the thrust. Furthermore, a 3D-printed prototype robot based on the described contents is manufactured. This research is expected to provide insights for the structural design of propeller-based wall-climbing robots.

Keywords: *Wall-climbing robot, Propeller thrust force, Wheel-based driving system, CFD simulation*

1. Introduction

Wall climbing robots have demonstrated the potential to replace humans in various industrial sectors accompanied by working in hazardous conditions, such as bridge inspection[1], cleaning of high-rise building exteriors[2], wind turbine inspection[3], firefighting[4], and rescue[5]. Therefore, numerous studies are being conducted to advance wall-climbing mechanisms.

A variety of wall climbing robots have been designed using different adhesion techniques, including vacuum adhesion methods utilizing a suction cup[6-7], footpad using an adhesive coating method[8-9], adhesion based on the principle of magnetism[10-12], bio-inspired methods that mimic nature[13-14], and climbing methods using rope support[15]. While these platforms enhance adaptability in different settings, they can be sensitive to surface properties and environmental changes, limiting their universal applicability in industry. Their complex actuation and controls can also pose challenges in real-world industry environments.

Manuscript Received: September. 24, 2024 / Revised: September. 29, 2024 / Accepted: October. 4, 2024
Corresponding Author: dongha@seoultech.ac.kr
Tel: +82-2-970-7287
Professor, Department of MSDE, Seoul National University of Science & Technology, Korea

Propeller-based wall-climbing robots can overcome the aforementioned challenges. Unlike other platforms, propeller-based robots are less sensitive to surface characteristics and environmental factors, enhancing their universal applicability. Moreover, like drones, these robots use propeller thrust for wall attachment, which alleviates the need for intricate actuation control. Furthermore, a wheel-based driving mechanism is essential for quick and dynamic movement in hazardous industrial environments.

This combination of technologies was featured in the wall climbing robot, Vertigo[16], co-developed by Disney Research and ETH Zurich. Subsequent studies have been conducted on various propeller-based wall climbing robots using Vertigo as a reference. Nevertheless, there is a dearth of research on the structural design of robots with operating principles based on Vertigo. This paper aims to fill this gap by presenting detailed mechanical designs and a simulation method to analyze the thrust of a propeller-based wall-climbing robot integrated with a wheel driving system. This study

2. Mechanical Design

2.1 Overall Specification

The weight of the prototype robot based on the mechanical design illustrated in Figure 1 is $0.84\,kg$, excluding the battery. We assume that the driving and control motors are powered through wire connections from an external source. The structure of the robot consists of a body frame, two propeller driver units, and a wheel-based locomotion structure, which includes suspension, and steering. The propeller driver unit is comprised of several components to obtain the multiple direction of thrust. The components of this unit include a $2200\,KV$ brushless driving motor, a $155\,mm$ 2-blade propeller, a tiltable fan guard, a motor mounting member, a roll tilt angle control motor, and a pitch tilt angle control motor. With this drive unit, the robot can perform basic movements such as moving forward or backward, as well as climbing walls. Additionally, two independent steer angle control motors are employed for steering capabilities. More detailed specifications of the robot are shown in Table 1. The propeller height is the distance between a wall and the propeller center.

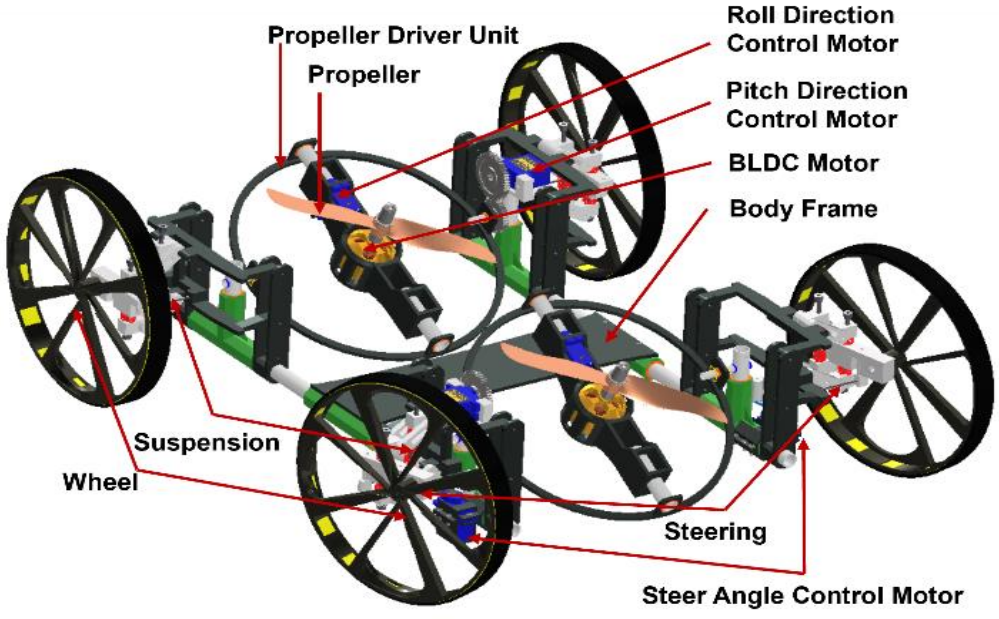

Figure 1. 3D-CAD modeling of the robot

Table 1. Design specification of the prototype robot

Specification	Value
Body Size	$(465 \times 368 \times 152)\ mm$
Wheel Diameter	$146.5\ mm$
Mass (m)	$0.84\ kg$
Steering Angle	$-18° \sim +18°$
Propeller Driver Unit	Roll: $-50° \sim +50°$
Tilt Angle	Pitch: $-30° \sim +30°$
Propeller Height (H)	$86\ mm$
Propeller Diameter (D)	$155\ mm$
Propeller Pitch	$4.5\ inches$
Brushless Motor	$2200\ KV$ ($2563\ \text{rad/s}\ @\ 11.1\ V$)

2.2 Body Frame

Minimizing weight remains a primary challenge in developing wall-climbing robots that can navigate vertical surfaces stably. By reducing weight, movement efficiency is enhanced, and the stress on the climbing mechanism is diminished, extending the robot's lifespan. To meet this objective, we adopted an H-shaped chassis frame made of lightweight, high-strength carbon pipes in the robot's foundational structure as illustrated in Figure 2. Furthermore, to reduce the robot's overall size and eliminate unnecessary space, we designed a concave body plate. This plate adjusts both the spacing between the fans and provides adequate space for the embedded system.

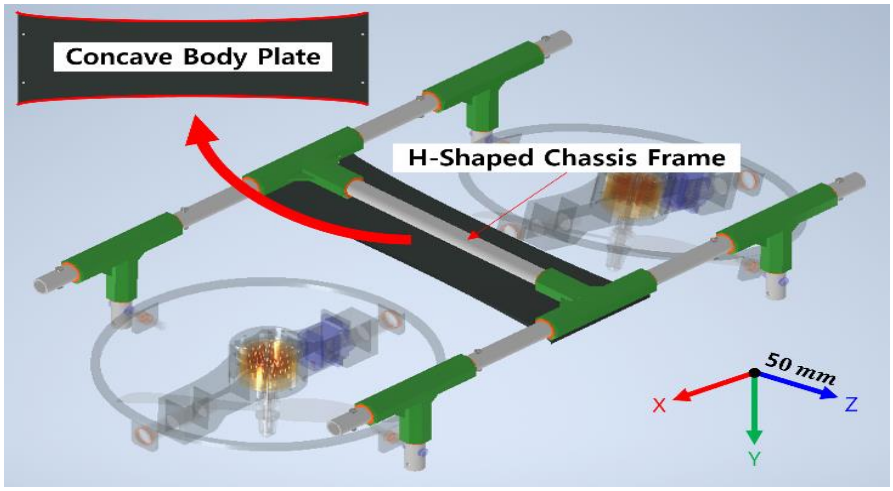

Figure 2. Bottom view of 3D cad model of the body frame

2.3 Propeller Driver Unit System

The proposed robot is equipped with two propeller driver units for driving. Each of these units is uniformly comprised of a $2200\ KV$ brushless motor, a 2-blade propeller with a diameter of $155\ mm$, a tiltable fan guard, a motor mounting member, and two control motors for tilt operations of roll title angle, as illustrated in

Figure 3(a). For multi-degree tilting of the propeller disk, two control motors with different tilting directions are utilized for each propeller driver unit. As shown in Figure 3(b), the control motor mounted inside the motor mounting member facilitates tilting in the roll title angle, ranging from $-50°$ to $+50°$. Furthermore, the control motor shown in Figure 3(c) allows them to control the pitch tilt angle from $-30°$ to $+30°$. So, it plays a pivotal role in achieving dexterous movement for the robot. Furthermore, As shown in Figure 3(d), the motor mounting member has a curvilinear design that serves to control the distance between itself and the ground surface and reduce component weight. Additionally, strategic vents have been employed to counteract the heat generated by the brushless motor.

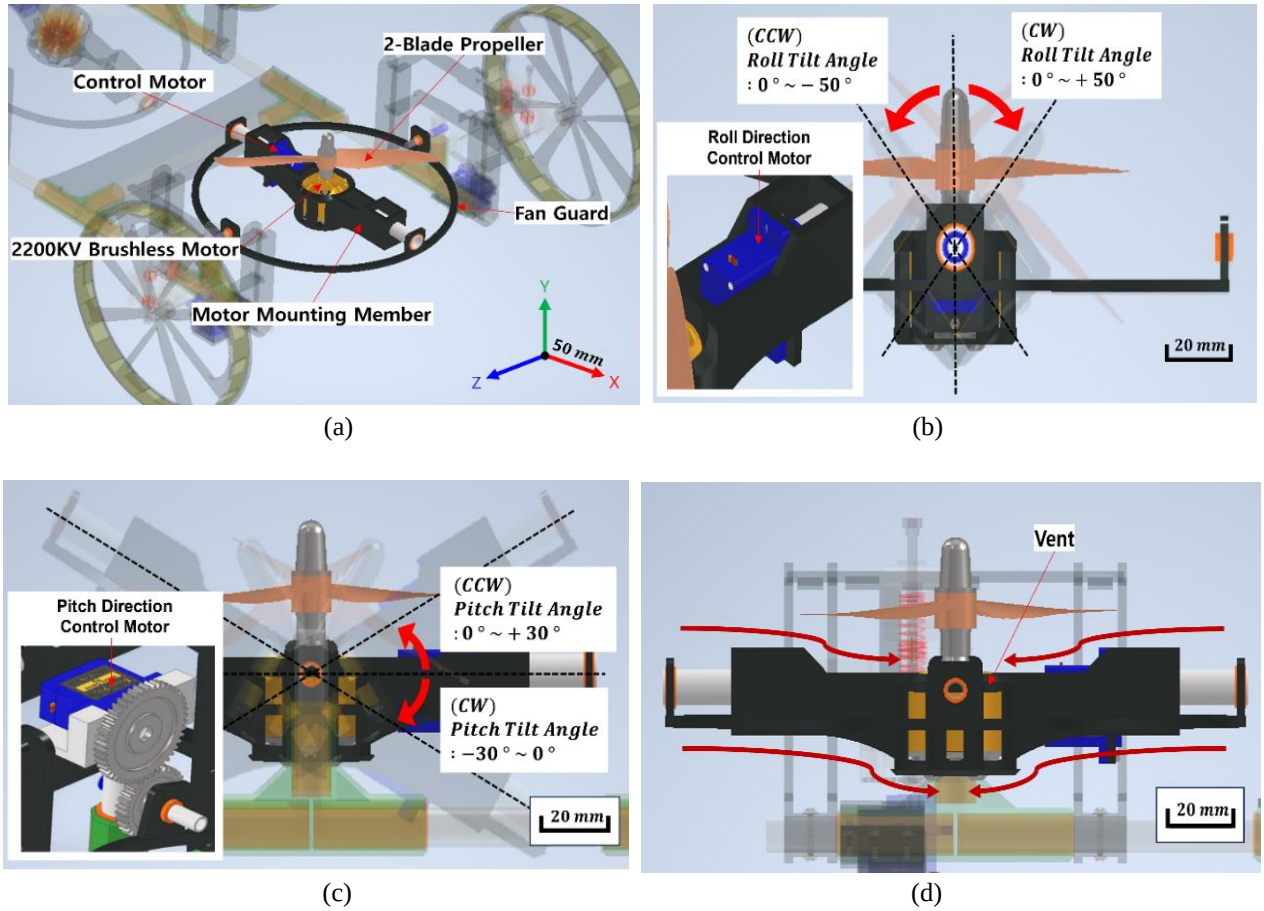

Figure 3. 3D CAD model of the propeller driver unit.
(a) Overall view, (b) Roll tilt angle control system for propeller disk,
(c) Pitch tilt angle control system for propeller, (d) Lateral view

2.4 Wheel-Based Driving Mechanism

We designed a rim with a large diameter (146.5 mm) as illustrated in Figure 4 to reduce rotational inertia and weight while enhancing driving stability. To reduce the weight of the rim, we introduced evenly spaced holes on its side. Additionally, to enhance wall-riding stability by increasing the wheel's contact area, A sponge layer is employed with a silicon tire to expand the wheel's contact area and aid in reducing the stress exerted on the rim due to the vehicle's load.

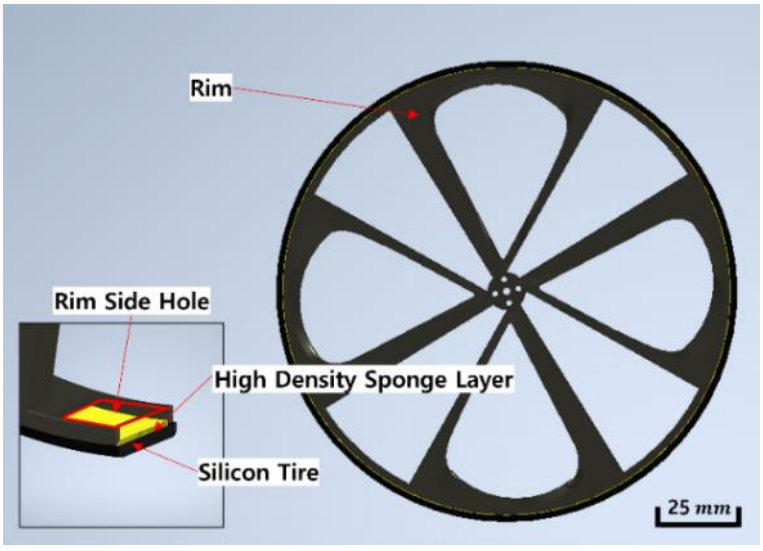

Figure 4. Overall and cross-sectional view of 3D cad model of the wheel

The wheel for the driving of the robot is connected to both the steering and suspension systems for driving safety. The dual steering rod system, which mimics the Ackermann steering geometry as illustrated in Figure 5[17], is designed. Therefore, the steering capability of the vehicle is enhanced by adjusting an outer wheel angle (δ_0) and an inner wheel angle (δ_1), following circles of different radii. This system, depicted in Figure 6, simplifies steering, prevents abrupt angle changes due to obstacles, and avoids interference with the suspension. This design guarantees consistent steering and allows the vehicle to follow a unique centrifugal circular trajectory.

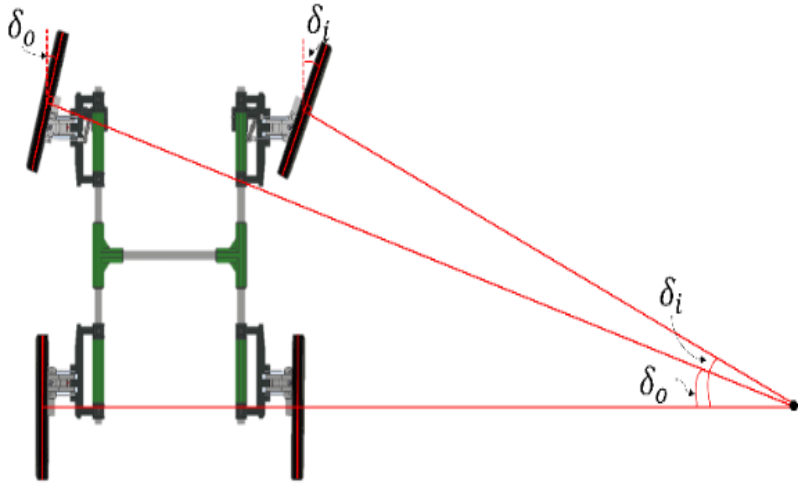

Figure 5. Ackermann steering geometry of the presented robot with a toe angle of δ_o for the left wheel and δ_i for the right wheel

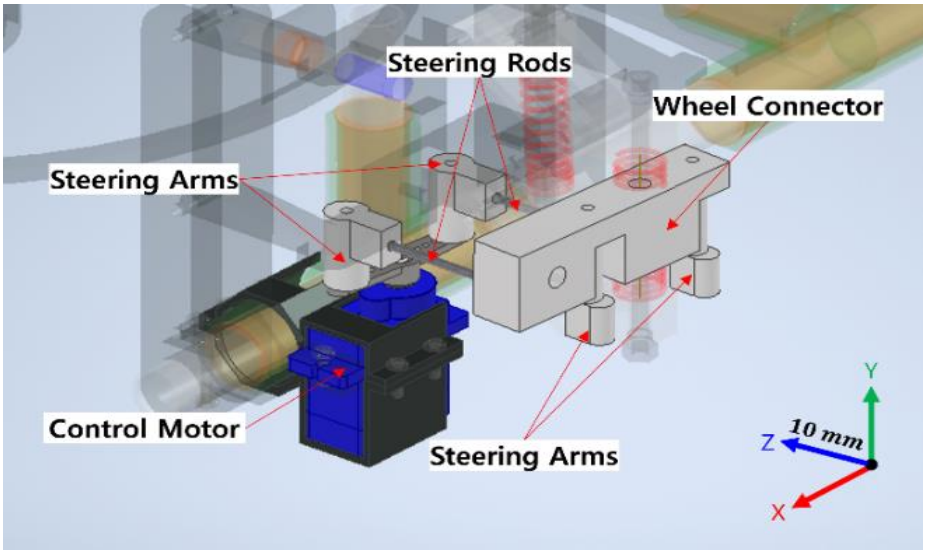

Figure 6. Overall view of 3D cad model of the steering system

Also, the suspension system, illustrated in Figure 7, is equipped to get stable driving. The design minimizes a flipping over, especially at high speeds. The system is divided into three independent shock absorber units for adaptability and performance on diverse terrains.

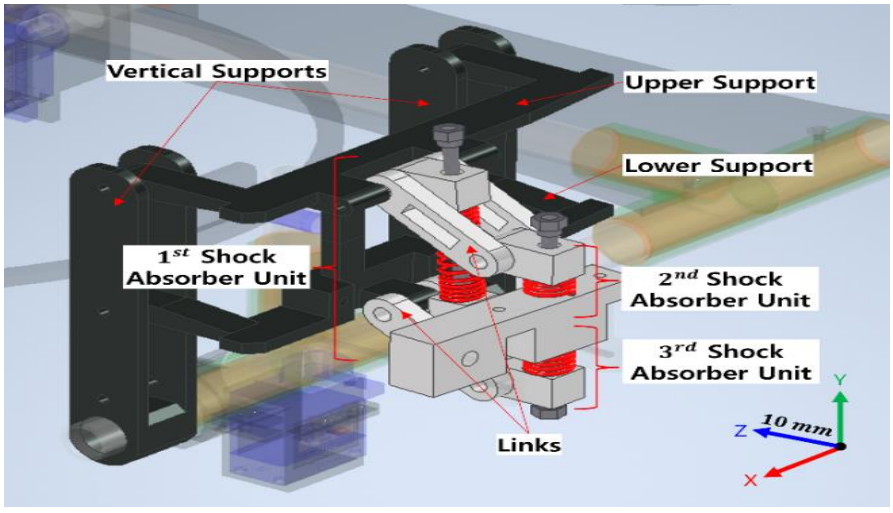

Figure 7. 3D Overall view of 3D cad model of the suspension system

3. CFD-Based Thrust Optimization Design

3.1 Model Design

The thrust analysis is one of the important factors in the operating efficiency of the robot. The propeller height (H), the distance between the wall and the center of the propeller, could be an independent variable design component to analyze it. Therefore, the CFD (Computational Fluid Dynamics) simulation was performed. Overall domains and boundary conditions of the simulation were modeled as shown in Figure 8(a).

In this study, an inlet surface is set to a side space of a stationary surface that is near the wall surface, which is considered as a contact surface with the wheels of the robot. Therefore, the inlet surface has the same shape as a circular band. The reason why the inlet is set in this way is, for the actual propeller-based wall-climb robots, an upstream that flows into the propeller comes from the surface parallel to the central axis of a rotating domain as illustrated in Figure 8(b). The dimension of the rotating domain and the stationary domain is designed based on the diameter of the propeller (D). The rotating domain was modeled like a thin cylinder that surround the propeller. The stationary domain has enough space between the wall surface and an outlet surface not to affect the downstream analysis results of the propeller. Also, this domain was designed to consider the variable distance from the center of the rotating domain to the wall space, denote as H, as shown in Figure 8(c), since the propeller height is a dependent variable in this simulation.

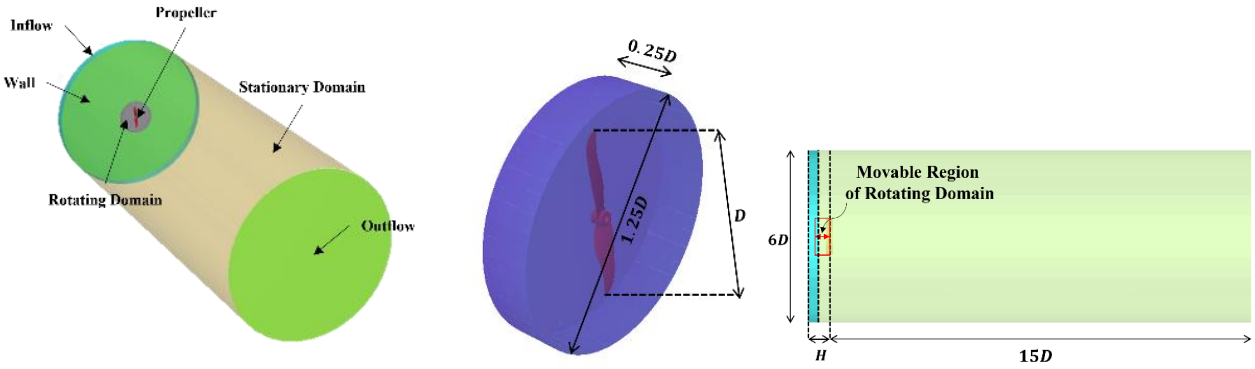

Figure 8. Domain and boundary condition of simulation.
(a) overall domain and boundary conditions, (b) size specification of rotating domain,
(c) size specification of stationary domain and inlet

The specifications boundary conditions of the simulation are set as shown in Table 2. The mass flow rate of the outlet was referred to as the value derived from the initially designed CFD simulation. The rotational speed of the propeller is the ideal angular velocity when the recommended about 11.1 voltage from the specification sheet of the motor used in the prototype robot is applied.

Table 2. Simulation conditions

Specification	Value
Mass Flow Rate	11.03 kg/s
Air density	1.177 kg/m^3
Dynamic Viscosity	$1.85 \cdot 10^{-5}$ m^2/s
Rotational Speed	2563 rad/s

3.2 Simulation Result

Under the same simulation conditions, the simulation was conducted for five different values of H. If the runtime of the simulation is set to enough, observations of streamlines and propeller thrust could be challenged. Therefore, all the simulations ran for 0.2 sec virtually. At the same time, the observations of shape and data were conducted consistently with time steps at 0.1 $msec$ intervals. As a result, even though the inlet position

was set on the side of the stationary domain, a stable streamline was observed in the direction of the outlet surface, as illustrated in Figure 9.

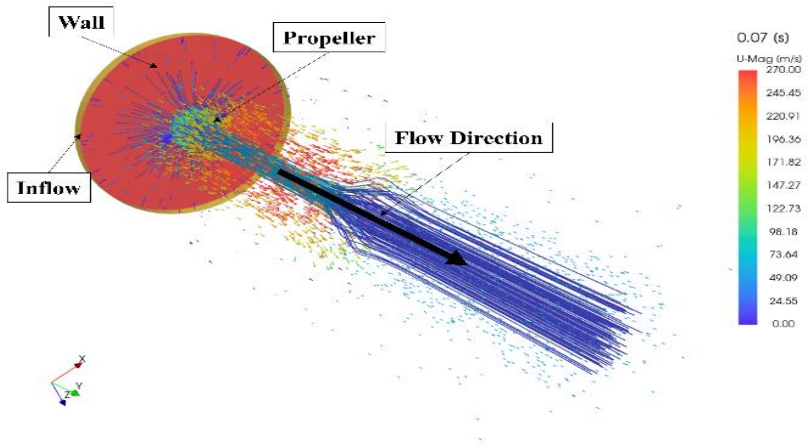

Figure 9. Result of streamlines visualization generated by propeller rotation at $0.07\ sec$

The result of the propeller's thrust, measured for each simulation at different running time intervals, is presented in Figure 10. For easier interpretation, the fluctuated original data was processed with polynomial regression to represent a trendline. From this simulation result, an increasing trend in thrust was clearly observed as H elevates.

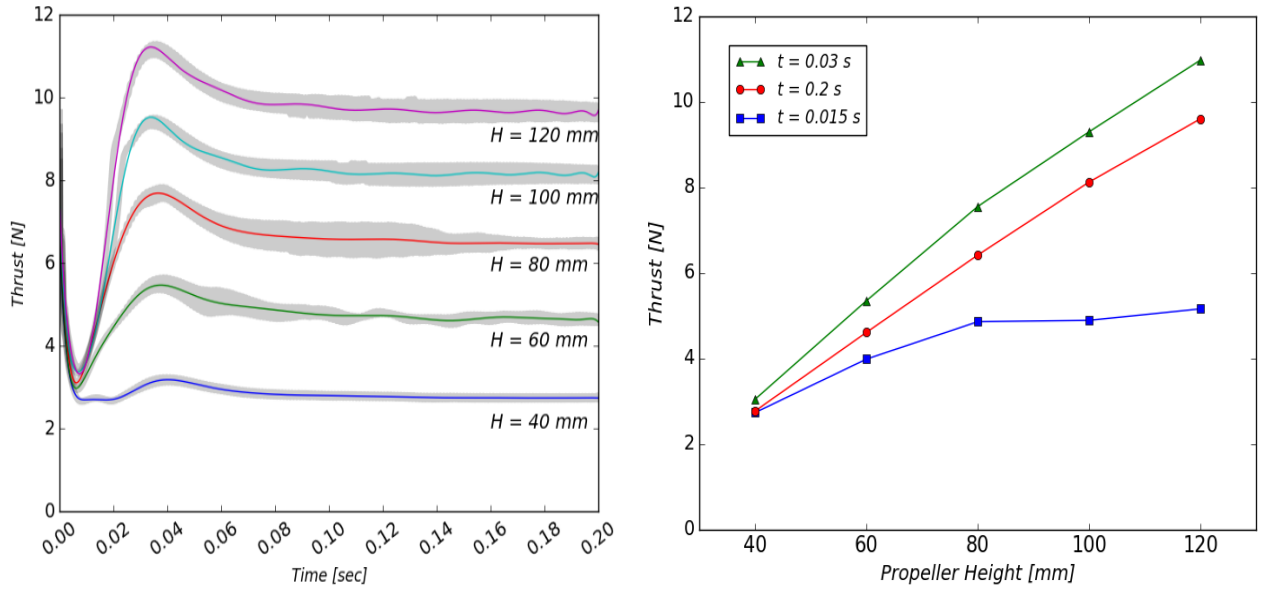

(a) (b)

Figure 10. Simulated results of thrust for different propeller heights (H)

(a) temporal thrust response for various heights (gray areas: band of the simulation results, linear plots: polynomial regression trendlines), (b) thrust variation against propeller height

3.3 Validation of Simulation Analysis

To verify the validity of the simulation analysis, the simulation results for large H were compared with the semi-empirical dynamic propeller thrust equation for an open-space in equation (1). This equation, which integrates empirical data to refine theoretical predictions, offers a framework to predict the propeller's thrust performance. The equation is known to underestimate 15-30% lower than actual measurement data[18].

$$Thrust = 4.392 \cdot 10^{-8} \cdot RPM \cdot \frac{d^{3.5}}{\sqrt{pitch}} \cdot (4.233 \cdot 10^{-4} \cdot RPM \cdot pitch - V_0)$$
$$d = propeller\ diameter\ (inch)$$
$$pitch\ = propeller\ pitch\ (inch) \quad (1)$$
$$RPM\ = propelle\ rotational\ speed\ (rpm)$$
$$V_0 = propeller\ forward\ airspeed\ (m/s)$$

The thrust is calculated to be $13.26\,N$ for RPM of $24484.4\,rpm$, $pitch$ of $4.5\,inches$, d of $6.1\,inches$, and V_o of zero. The actual measured thrust is estimated 15% to 30% higher to be between $15.60\,N$ and $18.95\,N$. Under the conditions in Section 3.1, the simulated thrust converges to about $18\,N$ when H is $400\,mm$ and $800\,mm$. In this case, where the simulation domain approaches an open space, the results are illustrated in Figure 11. The validity of the simulation model is verified with the moderate error range of -0.5% to 15.37%.

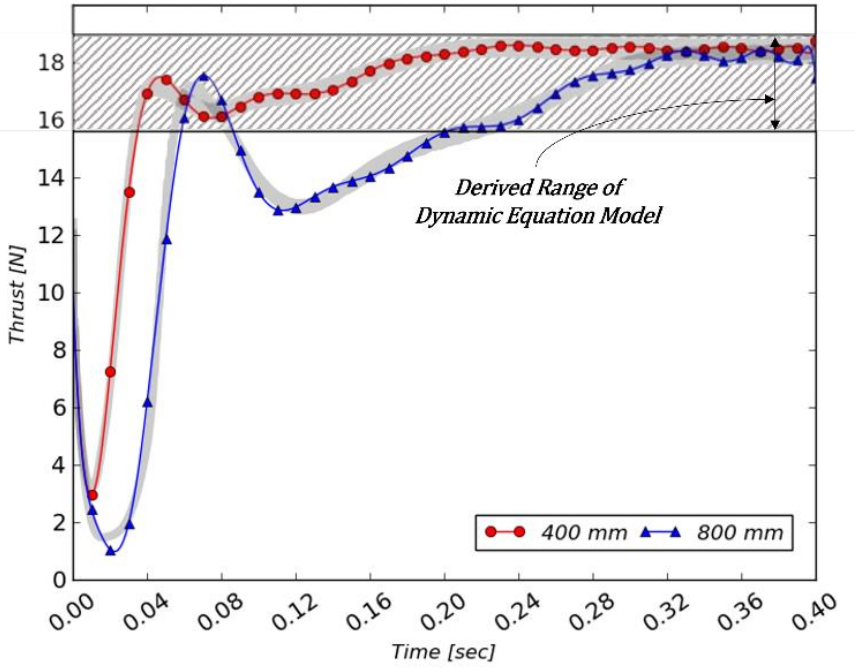

Figure 11. Simulated results of thrust for propeller heights (H) in open-space condition (gray areas: band of the simulation results, linear plots: polynomial regression trendlines, crosshatch area: derived range of dynamic equation model).

3.4 Operation Conditions

The proposed wall-climbing robot employs two propeller drive units. Therefore, the simulation output of the force needs to be twice. To ensure stable driving with this thrust, specific conditions must be satisfied. Figure 12 depicts the free-body diagram (FBD) of the robot. The robot, with a weight is mg due to its mass (m) and the gravitational acceleration (g), adheres to the wall inclined at θ' degree, driving by tilting its propeller disk at an angle of θ with thrust force of T_{prop} for each propeller. Through this diagram, two critical conditions can be derived.

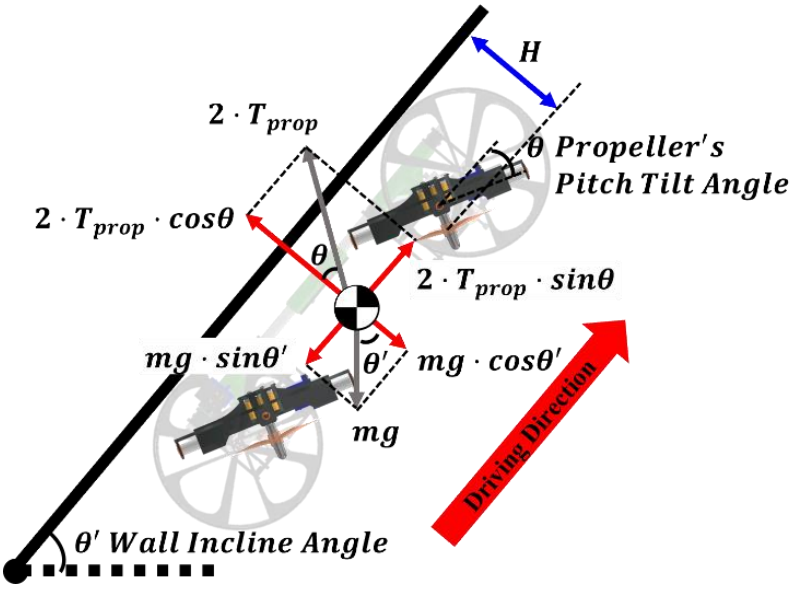

Figure 12. FBD of the wall climbing robot climbing an inclined wall

The first condition is that the force vector of T_{prop} perpendicular to the wall must be greater than the force acting in its opposite force vector due to the weight of the robot.

$$2 \cdot T_{prop} \cdot cos\theta > mg \cdot cos\theta' \tag{2}$$

The second condition is that the force vector of T_{prop} parallel to the wall, for driving in an adhered state, exceeds the force applied to its opposite force caused by the weight.

$$2 \cdot T_{prop} \cdot sin\theta > mg \cdot sin\theta' \tag{3}$$

Both equation (2) and equation (3) should be satisfied for all possible θ and $\theta'(0° < \theta' < 180°)$. Therefore, both equation (4) and equation (5) should be satisfied for a certain θ between $-30°$ and $+30°$ in the pitch tilt angle range as shown in Table 1.

$$2 \cdot T_{prop} \cdot sin\theta > mg \tag{4}$$
$$2 \cdot T_{prop} \cdot cos\theta > mg \tag{5}$$

When the pitch tilt angle is a maximum as shown in Table 1 ($\theta = 30°$), both equation (4) and equation (5) are satisfied with a minimum T_{prop}. Both conditions can be expressed as equation (6).

$$T_{prop} > mg \tag{6}$$

As a result, when equation (4) is satisfied, the proposed robot can stably drive on any wall angle (θ'). According to Figure 10, the minimum propeller height is $60\,mm$ to achieve T_{prop} greater than mg ($8.24\,N$). Therefore, the propeller height of the proposed wall-climbing robot was designed to be $86\,mm$, as shown in Table 1, considering the dynamic stability of the robot. A larger propeller height raises the center of the mass to degrade the driving safety of the robot.

4. Experiments

We fabricated the prototype of the proposed wall climb robot, as shown in Figure 13, using FullCure720[19] as the 3D printing material to verify the compatibility among components and reduce the weight of the body frame. The overall specifications of this prototype robot are described in Table 1 of Section 2.1.

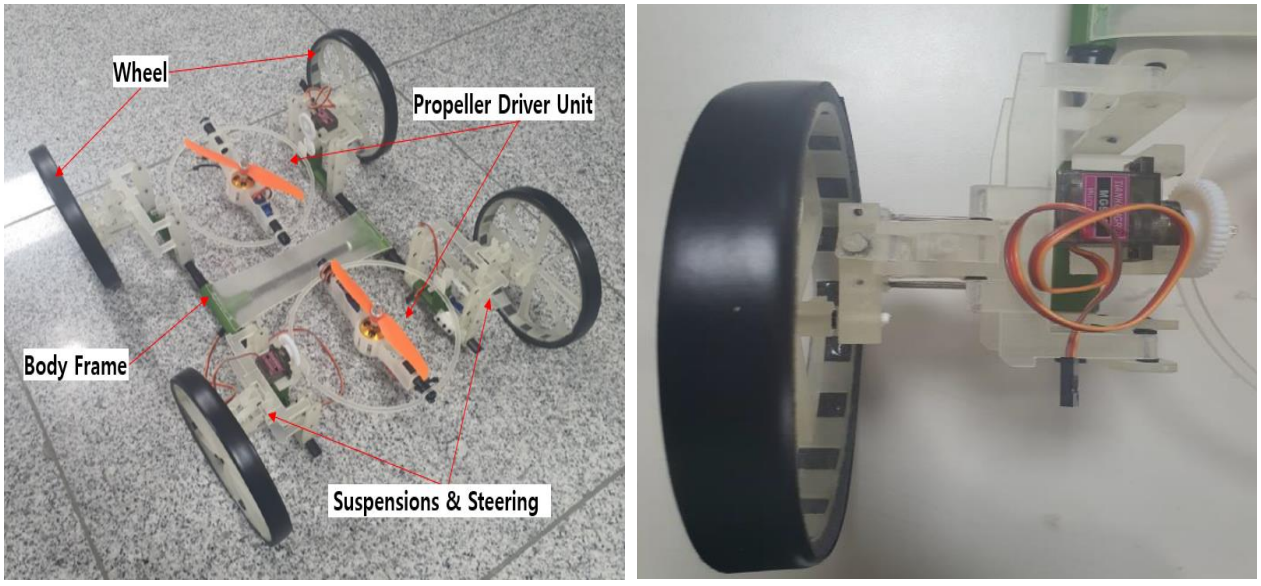

(a) (b)

Figure 13. 3D-Printed prototype of the robot
(a) overall view, (b) top view of the front wheel's suspension and steering structure

We conducted a driving test on a horizontal ground. When the prototype was driven with the thrust generated from only one propeller disc, the velocity was measured to be $1\,m/s$ with stable driving conditions, as shown in Figure 14. However, due to the limitation of implementation, an overhang driving test is not conducted.

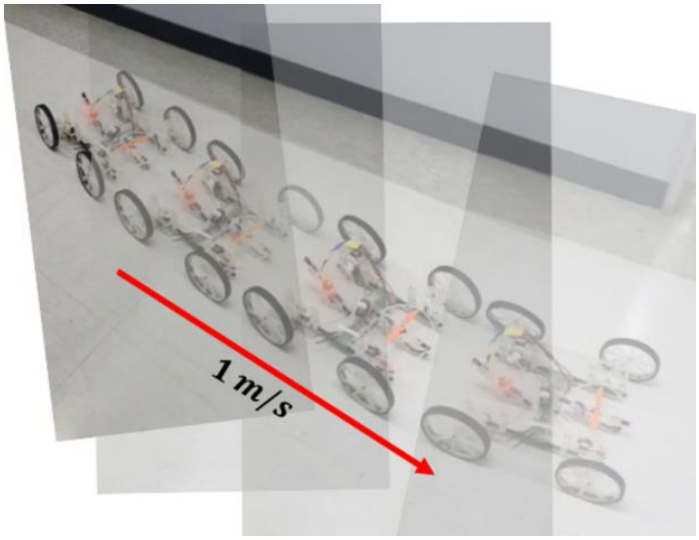

Figure 14. Driving test on a horizontal surface

5. Conclusion

In this study, we developed the mechanical structure and design of the propeller-based wall-climbing robot and introduced the CFD simulation model to optimize thrust depending on the height of the propeller. Through this model, we analyzed how the propeller height influences the thrust performance, which is the dependent variable. The result of the simulation, designed with the consideration of the actual upstream flow passes into the propeller driver unit, showed a notable increasing trend in thrust as the distance between the ground and the propeller increases, and verified the validity of the simulation by confirming dynamic propeller thrust equation. Furthermore, based on the proposed mechanical design and simulation, we fabricated a prototype robot using 3D printing. The prototype robot demonstrated stable driving on a horizontal ground with the thrust of its propeller disks without the additional wheel power. However, we were unable to conduct detail experiments such as the overhang driving test due to limitations in implementation. Therefore, further driving tests are needed for the wall with various surface angles including the overhang.

References

[1] S. T. Nguyen, A. Q. Pham, C. Motley, and H. M. La, “A Practical Climbing Robot for Steel Bridge Inspection,” IEEE Xplore, May 01, 2020. DOI: https://doi.org/10.1109/ICRA40945.2020.9196892

[2] T. Kim, Y. Jeon, S. Yoo, K. Kim, H. S. Kim, and J. Kim, “Development of a wall-climbing platform with modularized wall-cleaning units,” Automation in Construction, vol. 83, pp. 1–18, Nov. 2017. DOI: https://doi.org/10.1016/j.autcon.2017.07.004

[3] The Verge, "GE's Wind Turbine Inspection Robot", https://www.theverge.com/2012/6/13/3083141/ge-wind-turbine-robot.

[4] Wancheol Myeong, Kwang Yik Jung, and H. Myung, “Development of a fire-proof aerial robot system for fire disaster,” Aug. 2017.

[5] M. T. Pope and M. R. Cutkosky, “Thrust-Assisted Perching and Climbing for a Bioinspired UAV,” Lecture notes in computer science, pp. 288–296, Jan. 2016. DOI: https://doi.org/10.1007/978-3-319-42417-0_26

[6] Yanko Design, "Wall Climbing a Cinch", https://www.yankodesign.com/2008/03/05/wall-climbing-a-cinch/.

[7] H. Zhu, Y. Guan, W. Wu, L. Zhang, X. Zhou, and H. Zhang, “Autonomous Pose Detection and Alignment of Suction Modules of a Biped Wall-Climbing Robot,” IEEE-ASME Transactions on Mechatronics, vol. 20, no. 2, pp. 653–662, Apr. 2015. DOI: https://doi.org/10.1109/tmech.2014.2317190

[8] Y. Liu, H. Kim, and T. Seo, “AnyClimb: A New Wall-Climbing Robotic Platform for Various Curvatures,” IEEE/ASME Transactions on Mechatronics, vol. 21, no. 4, pp. 1812–1821, Aug. 2016. DOI: https://doi.org/10.1109/tmech.2016.2529664

[9] M. P. Murphy and M. Sitti, “Waalbot: An Agile Small-Scale Wall-Climbing Robot Utilizing Dry Elastomer Adhesives,” IEEE/ASME Transactions on Mechatronics, vol. 12, no. 3, pp. 330–338, Jun. 2007. DOI: https://doi.org/10.1109/tmech.2007.897277

[10] M. Eich and T. Vögele, “Design and control of a lightweight magnetic climbing robot for vessel inspection,” IEEE Xplore, Jun. 01, 2011. DOI: https://doi.org/10.1109/ICRA40945.2020.9196892

[11] W. Song, H. Jiang, T. Wang, D. Ji, and S. Zhu, “Design of permanent magnetic wheel-type adhesion-locomotion system for water-jetting wall-climbing robot,” vol. 10, no. 7, p. 168781401878737-168781401878737, Jul. 2018. DOI: https://doi.org/10.1177/1687814018787378

[12] F. ROCHAT, P. SCHOENEICH, OLIVIER TRUONG-DAT NGUYEN, and F. MONDADA, “TRIPILLAR: MINIATURE MAGNETIC CATERPILLAR CLIMBING ROBOT WITH PLANE TRANSITION ABILITY,” Infoscience (Ecole Polytechnique Fédérale de Lausanne), Aug. 2009. DOI: https://doi.org/10.1142/9789814291279_0044

[13] J. Liu, L. Xu, J. Xu, X. Wu, M. Wang, and L. Lu, “A Bio-inspired Wall-climbing Robot with Claw Wheels and Adhesive Tracks,” Aug. 2018. DOI: https://doi.org/10.1109/icinfa.2018.8812342

[14] Y. Liu, S. Sun, X. Wu, and T. Mei, “A Wheeled Wall-Climbing Robot with Bio-Inspired Spine Mechanisms,” Journal of Bionic Engineering, vol. 12, no. 1, pp. 17–28, Mar. 2015. DOI: https://doi.org/10.1016/s1672-6529(14)60096-2.

[15] W. Wang, B. Tang, H. Zhang, and G. Zong, “Robotic cleaning system for glass facade of high - rise airport control tower,” Industrial Robot: An International Journal, vol. 37, no. 5, pp. 469–478, Aug. 2010. DOI: https://doi.org/10.1108/01439911011063290.

[16] Disney Research, "VertiGo: A Wall-Climbing Robot," https://web.archive.org/web/20190208192644/https://www.disneyresearch.com/publication/vertigo.

[17] Racecar Engineering, "Tech Explained: Ackermann Steering Geometry," https://racecar-engineering.telegraph.co.uk/articles/tech-explained-ackermann-steering-geometry/.

[18] Tyto Robotics, "How to Calculate Propeller Thrust," https://www.tytorobotics.com/blogs/articles/how-to-calculate-propeller-thrust.

[19] BuildParts, "FullCure720 Material Information," https://www.buildparts.com/materials/fullcure720/.